Evaluation of vertical stress distribution in field monitored GRS-IBS structure

F. Gebremariam[1], B. F. Tanyu[2], B. Christopher[3], D. Leshchinsky[4], J. Han[5] and J. G. Zornberg[6]

[1]*Graduate Research Assistant, Department of Civil, Environmental, and Infrastructure Engineering, George Mason University, 4400 University Drive, Fairfax, VA 22030, USA, E-mail: fgebrema@gmu.edu*
[2]*Associate Professor, Department of Civil, Environmental, and Infrastructure Engineering, George Mason University, 4400 University Drive, Fairfax, VA 22030, USA, E-mail: btanyu@gmu.edu (corresponding author)*
[3]*Geotechnical Consultant, 210 Boxelder Lane, Roswell, GA 30076, USA, E-mail: barryc325@aol.com*
[4]*Adama Engineering and Professor Emeritus from University of Delaware, 12042 SE Sunnyside Rd., Suite 711, Clackamas, OR 97015, USA, E-mail: adama@geoprograms.com*
[5]*Professor, Department of Civil, Environmental, and Architectural Engineering, The University of Kansas, 2150 Learned Hall, 1530 W. 15th Street Lawrence, KS 66045, USA, E-mail: jiehan@ku.edu*
[6]*Professor, Department of Civil, Architectural, and Environmental Engineering, The University of Texas at Austin, 301 E. Dean Keeton, Room ECJ 9.227, Austin, TX 78712, USA, E-mail: zornberg@mail.utexas.edu*

Received 05 September 2019, revised 18 November 2019, accepted 19 December 2019, published 05 August 2020

ABSTRACT: This paper presents a case study of a geosynthetic-reinforced soil (GRS) integrated bridge system (IBS) in which the vertical stresses during and after construction were monitored via instrumentation. The purpose of the study was to evaluate the effects of reinforcement spacing, width of the beam seat, and seasonal variations on the vertical stresses measured in the field. The stress distribution observed in the field was also compared to the theoretically estimated stress distribution. The results showed that the bearing bed where the reinforcements are doubled is effective in reducing the applied stresses by about 1.8 to 5.4 times. The width of the beam seat controlled the magnitude of the applied stresses on the GRS abutment and the applied stress was vertically transferred all the way to the foundation level even in wider beam seats. A comparison between field recorded and theoretical stress values showed that the Boussinesq method provides a better estimate of the field vertical stress distribution than the approximate 2 : 1 method, although the 2 : 1 method provides more conservative stresses to be considered for design. Results from long-term monitoring indicated that vertical stress distribution in the GRS abutments was not significantly influenced by seasonal variations.

KEYWORDS: Geosynthetics, Vertical stress, Stress distribution, Geosynthetic reinforced soil (GRS), Integrated bridge system (IBS), Earth pressure cells, Vertical reinforcement spacing, Beam seat width, Seasonal variations

REFERENCE: Gebremariam, F., Tanyu, B. F., Christopher, B., Leshchinsky, D., Han, J. and Zornberg, J. G. (2020). Evaluation of vertical stress distribution in field monitored GRS-IBS structure. *Geosynthetics International*, **27**, No. 4, 414–431. [https://doi.org/10.1680/jgein.20.00004]

1. INTRODUCTION

Over the last nine years, the Federal Highway Administration (FHWA) has been promoting an approach for supporting bridges directly on geosynthetic reinforced soil (GRS) structures through a concept referred as Geosynthetic Reinforced Soil (GRS) – Integrated Bridge System (IBS) (Adams *et al*. 2011). It has been reported that this new system can help reduce construction time significantly as there is no need for deep foundations nor for curing time for concrete in conventional concrete abutments before the superstructure can be placed over the abutment (Adams *et al*. 2007; Bloser *et al*. 2012; Abernathy 2013; Budge *et al*. 2014; Saghebfar *et al*. 2016). Over the last 5 years, more than 200 abutments have been constructed in the United States using GRS-IBS structures rather than conventional reinforced concrete abutments (FHWA 2019; Sachin and Mehari 2019).

One of the unique features of this system is that construction of a GRS-IBS blends the bridge superstructure with the integrated approach through a jointless connection, which is intended to mitigate a potential bump at the junction of the bridge deck and the approach fill (Helwany *et al*. 2003; Adams *et al*. 2011, 2012;

Talebi *et al*. 2017). Although the term 'GRS-IBS' refers to a specific construction method, reinforced soil structures have been used to construct load-carrying bridge abutments (i.e. bridges supported directly over the mechanically stabilized earth (MSE) wall using spread footing foundations) for the past several decades (Berg *et al*. 2009). MSE technology has been around since 1966, initially involving steel reinforcement and shortly after using geosynthetic reinforcement, with thousands of walls having been constructed in the U.S. (Christopher 1993; Abu-Hejleh *et al*. 2003; Wu *et al*. 2006; Tanyu *et al*. 2008; Sachin and Mehari 2019). Both GRS-IBS and MSE structures are composed of alternating layers of compacted, high-quality granular backfill aggregate and reinforcements. The primary differences between GRS-IBS and MSE are the maximum spacing requirements between the vertical reinforcements (S_v) and the superstructure's integration with the roadway approach. In GRS-IBS, the maximum allowed vertical reinforcement spacing is limited to 0.3 m, whereas in MSE it is limited to 0.8 m. Additionally, GRS-IBS requires construction of a reinforced foundation and a bearing bed zone, where the vertical spacing between the reinforcements is reduced in half (e.g. doubling the density of reinforcements) along the zone underneath the superstructure. Also, the reinforced fill gradation requirements are more restrictive in GRS-IBS guidelines than those required by AASHTO (2016) and FHWA (Berg *et al*. 2009) for MSE walls.

Estimation of the vertical stress distribution in GRS structures (for both GRS-IBS and MSE structures) is a very important design element, as these estimations are needed to assess both internal and external stability. While this topic has been of interest to researchers, actual field information on vertical stress distribution values is limited. A summary of previous research findings from field-monitored GRS-IBS and MSE projects, in which vertical stress values were obtained from instrumentation, is outlined below.

In some structures, it was observed that the vertical stress from superstructure is transferred all the way to the foundation of the GRS structure. This observation was reported by Morrison *et al*. (2006); Vennapusa *et al*. (2012); and Budge *et al*. (2014), where the researchers investigated the stress distribution on GRS-IBS and MSE structures reinforced with geosynthetics (woven geotextiles and geogrids) with a vertical spacing of 0.2 to 0.5 m. In all the evaluated structures, the reinforcements were frictionally connected to the facing. The height of the structures varied from 1.2 to 7 m and the superstructure loads (dead loads on GRS abutments and applied surcharge on a full-scale MSE test wall) were between 35 and 356 kPa. Talebi *et al*. (2017) looked at the vertical stress distribution within the foundation of the GRS specifically and stated that the stresses bearing pressure below the foundation do not distribute uniformly or follow a trapezoid shape, as is assumed in the existing design guidelines. The authors also stated that the reinforced soil foundation behaved in a flexible way under applied loads except in the proximity of the facing of the abutment.

In some structures, it was observed that the vertical stresses were higher close to the facing of the structure. This observation was emphasized by Yang *et al*. (2012), which focused on evaluating an MSE structure reinforced with geogrids at a vertical spacing ranging from 0.4 to 0.6 m. The reinforcements were mechanically connected to the facing elements. The height of the structure ranged between 1.95 and 6 m and the uniformly distributed load from road pavement was approximately 7 kPa. As explained by Yang *et al*. (2017), the vertical stress was higher close to the facing due to the resistance of the reinforced soil to the lateral earth pressure from behind. The mechanical connection of the facing elements could also account for this stress distribution, unlike the case of frictional connections used in GRS-IBS structures.

In some structures, the vertical stresses were smaller (by as much as 45%) close to the facing of the structure. This observation was reported by Desai and El-Hoseiny (2005) and Jiang *et al*. (2015), both of which focused on evaluating MSE retaining walls reinforced with geogrids at vertical spacings ranging from 0.3 to 0.9 m. The reinforcements were mechanically connected to the facing and the height of the structure ranged from 5 to 12.2 m. According to the researchers, the vertical stress along the facing was smaller because of the relative movement between the backfill and reinforcement close to the facing.

The results from earth pressure cells was found to match well with theoretical calculations as reported for a number of structures. Saghebfar *et al*. (2016) observed that the vertical stresses measured in the field using earth pressure cells due to the self-weight of the backfill matched well with theoretically calculated stresses, and the stresses measured close to and away from the facing were the same. The maximum stress measured in the abutment was found to be less than the bearing pressure allowed in GRS-IBS guidelines (Adams *et al*. 2011). However, other researches showed that the stress data from earth pressure cells were lower (Yang *et al*. 2017) and higher (Budge *et al*. 2014) than theoretically calculated vertical stresses. The researchers indicated that these discrepancies were most likely due to arching of the backfill material over the earth pressure cells as well as possibly inaccurate or missing calibration of the pressure cells.

In all GRS structures (both GRS-IBS and MSE), vertical stresses are typically derived from the self-weight of the backfill used to construct the abutment, the superstructure placed over the abutment, and the transitional loads that occur after construction (Berg *et al*. 2009). Results from the previously cited studies also make evident that the actual vertical stress distribution depends on the characteristics of the backfill, reinforcement, facing element, facing connections, as well as the interactions between these components. Although the estimation of loads induced by self-weight has been estimated consistently for all GRS structures, the methods used to estimate the loads from superstructure are different for GRS-IBS and MSE structures (Berg *et al*. 2009; Adams *et al*. 2011). In the design of generic MSE structures, the vertical stress distribution is calculated using the approximate 2 : 1

method as used by FHWA (Berg *et al.* 2009) and AASHTO (2016), while the GRS-IBS vertical stress distribution is calculated using the Boussinesq (1985) method (Adams *et al.* 2011). As discussed below, the Boussinesq method is based on the theory of elasticity, while the 2:1 distribution is an approximation of the Boussinesq solution (Perloff and Baron 1976; FHWA 2006).

The approximate 2:1 method estimates the stress distribution for a footing load, as follows

$$\Delta\sigma_v = Q/D(L+Z) \tag{1}$$

$$D = (b-2e) + Z \text{ for } Z \leq Z_1 \tag{2}$$

$$D = d + \frac{(b-2e)+Z}{2} \text{for } Z > Z_1 \tag{3}$$

$$Z_1 = (2\times d) - b \tag{4}$$

where $\Delta\sigma_v$ is the distributed vertical stress from the superstructure load, Q is the load on isolated footing, D is the effective width of the applied load at a given depth, L is the length of the footing, Z is depth of stress point below footing, Z_1 is the depth at which the effective width intersects the back of the wall facing, d is the horizontal distance between the facing and center of the footing width, b is the width of the footing, and e is eccentricity of footing load.

The Boussinesq method estimates the stress distribution as follows

$$\Delta\sigma_v = (q/\pi)\times(\alpha + \sin(\alpha)\cos(\alpha+2\beta)) \tag{5}$$

where $\Delta\sigma_v$ is the distributed vertical stress from the superstructure load, q is the surcharge pressure, and α and β are inclination angles for points of interest located at a horizontal distance from the centerline of the footing and depth (Z) from the width of the beam seat where the bridge surcharge is applied.

The approaches described above provide different estimates of the vertical stress distribution. The focus of the present paper was to provide insight on the vertical stress distribution within a field monitored by GRS-IBS. Rather than an MSE structure, a GRS-IBS was selected partly because there are two different reinforcement zones in these systems (i.e. primary reinforcement and bearing bed zones), which also provided an opportunity to evaluate the vertical stress distribution as a function of spacing between reinforcements. Furthermore, recent research conducted on GRS-IBS via field monitoring programs did not investigate the effects of vertical reinforcement spacing, beam seat width, and seasonal variations on the vertical stress distribution in the abutment, nor did they compare the stresses measured in the field with those estimated using the theoretical stress distribution methods provided in Equations 1–5. A unique aspect of the research described in this manuscript is the similarity in size of the GRS-IBS constructed in this study to the mini-piers constructed by the Federal Highway Administration (FHWA) at their Turner Fairbank Highway Research Center (TFHRC). Mini pier tests involve large scale laboratory load tests on a square column of soil reinforced soil using horizontal geosynthetic reinforcement layers that extend over the area of the column. The mini-pier tests conducted at the TFHRC are significant, as they were used by the FHWA as the basis for the design of all GRS-IBS structures constructed in the U.S. and the recommendation to use Equation 5 to estimate the vertical stress distribution (Adams *et al.* 2011).

The GRS-IBS structure used in this study was constructed by the Virginia Department of Transportation (VDOT) agency as support for a new bridge. The structure included 29 earth pressure cells (EPC) installed in both abutments. Additionally, one EPC was installed in a wooden box with a gravel base and cover outside the abutment, primarily to provide a control with a known stress and evaluate the seasonal effects on pressure measurements in the field. The study involved an extensive evaluation program to capture the vertical stress distribution estimated from the EPCs: (1) during construction via staged loading, (2) at the end of construction to evaluate self-weight, (3) after the placement of the superstructure, and (4) after the abutment was opened to traffic via truck loading. According to Adams *et al.* (2011), GRS-IBS achieves a composite behavior when the reinforcement spacing is kept at 0.3 m or less. As the reinforcement spacing increases beyond this threshold, the degree of composite behavior is reported to decrease. To understand the impact of reinforcement spacing on stress distribution, one of the abutments was loaded during construction (i.e. staged loading) and the load response obtained from the EPCs installed in the primary reinforcement zone ($S_v = 0.2$ m) was compared to the measurements from the EPCs installed in the bearing bed zone ($S_v = 0.1$ m). The other abutment was not loaded during construction, so the effect of staged loading on the magnitude of the stress distribution from one abutment could be compared with the other abutment to assess the effects of staged loading on the overall stress distribution within the abutment.

In the design of GRS-IBS, the bridge beam seat is considered a platform for distributing the superstructure loads to the GRS abutment (Adams *et al.* 2011). The GRS-IBS constructed for this study was designed to have a beam seat width of 0.6 m on one abutment and 1.2 m on the other, which enabled the research team to monitor the effect of beam seat width on the stress distribution from superstructure loads. Additionally, the stress distribution due to superstructure loads was compared with the theoretical stress distribution (as described in Equations 1–5).

After construction, the bridge superstructure was loaded four times in one year using a truck, and the stress distribution within both abutments was monitored to capture effects of seasonal variations. Furthermore, the long-term stress data obtained from the control EPC installed outside the GRS-IBS was used to assess the sensitivity of measured stresses to changes in weather conditions.

2. SELECTION OF EARTH PRESSURE CELLS

In the field monitoring program, a vibrating wire EPC capable of measuring pressure in the range of 0 to 300 kPa was evaluated for measuring vertical stresses in the GRS abutment. This specific EPC was considered based on the suitability of its size and shape for this project, as well as its success in generating reliable data in previously monitored GRS-IBS and MSE structures that were similar to the field monitored GRS-IBS investigated in this study. Two commercially available EPCs were tested in the geotechnical engineering laboratory at George Mason University (GMU), prior to construction of the GRS-IBS, to select the EPC to be used in the field. The details of these experimental tests are presented in this section.

2.1. Earth pressure cells and principles of operation

The EPCs used in this study consisted of two welded circular stainless-steel plates, 230 mm in diameter, between which hydraulic fluid was contained. When a load is applied on the plate, pressure is generated in the fluid. The pressure is then converted to an electrical signal by a vibrating wire pressure transducer located inside a housing that is connected to the plates by a steel rod. The pressure transducer is connected by an electric cable to a readout device (datalogger). A thermistor to measure the temperature at the time pressure measurements are taken was also situated inside the housing.

Depending on the type of readout device used, the data from the vibrating wire EPCs is expressed in digits or frequency. Digits are calculated as

$$\text{Digits} = \left(\frac{1}{\text{Period (seconds)}}\right)^2 \times 10^{-3} \tag{6}$$

or

$$\text{Digits} = \frac{(\text{Frequency (Hz)})^2}{1000} \tag{7}$$

Digits or frequency readings are then converted to pressure (P), as follows

$$P = (R_1 - R_0) \times G + (T_1 - T_0) \times K \tag{8}$$

where, R_1 is the current digit (frequency) reading, R_0 is the initial digit (frequency) reading, G is the calibration factor, T_1 is the current temperature reading, T_0 is the initial temperature reading, and K is the thermal factor.

A concern when using this type of instrument with granular backfill is the effect of point loading from particles in the backfill. If this loading occurs, it creates a non-uniform loading condition leading to stress measurements that do not reflect the actual stress distribution. Before field construction was initiated, the two different types of EPCs were evaluated in the laboratory to assess their suitability for use with granular backfill.

The EPC referred to herein as Model A had a thin plate (6 mm), whereas Model B had two thick plates (plate thickness was not reported by the manufacturer), as shown in Figure 1a. According to the manufacturer of Model B, the thicker plates reduce the effect of point loading from coarse aggregates. However, the thicker plates also make this model more expensive than Model A, which consequently necessitated a comparison between the two instruments, as the difference in cost

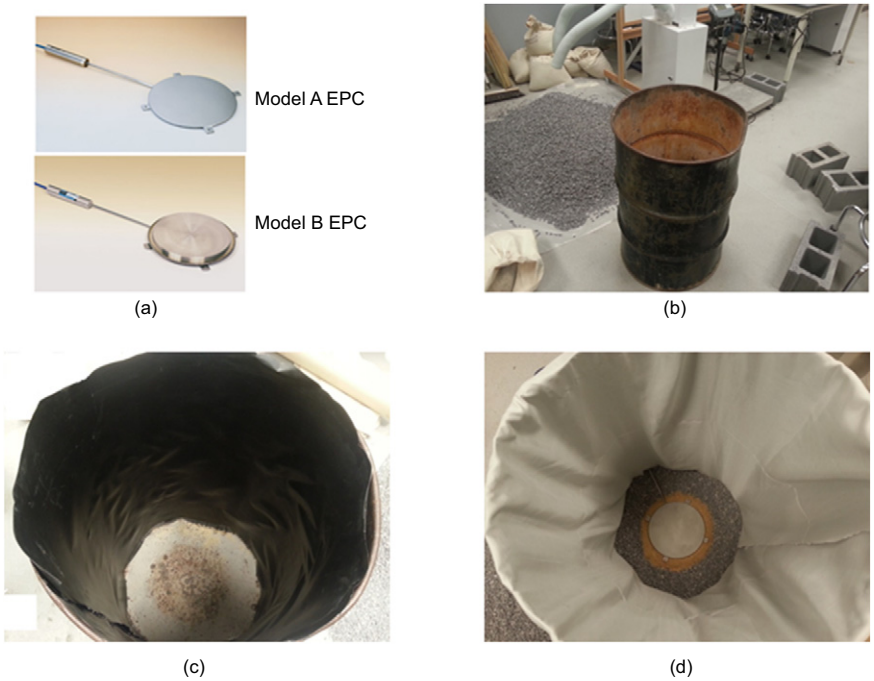

Figure 1. Experimental set-up used to test the suitability of two different EPCs: (a) photos of the models, (b) metal drum and aggregate used, (c) retrofitting the bottom and sides of the drum with a metal plate and geomembrane respectively, and (d) placement of satin fabric on top of the geomembrane to reduce side wall friction. *Note*: Figure 1d shows the placement of the Model A EPC at the bottom of the drum over the aggregate with placement of sand right underneath the EPC

affected the number of EPCs that could be utilized in the field.

2.2. Backfill material used to test the earth pressure cells in the laboratory

The backfill material used to test the EPCs in the laboratory was consistent with the backfill material to be used in the construction of the field monitored GRS-IBS. AASHTO No. 8 aggregate that meets the backfill specification in design of GRS-IBS was selected for this study. According to USCS classification (ASTM D2487-18), this aggregate classifies as poorly graded gravel (GP) with no fines, having a maximum particle size of 12.5 mm. The target dry density of this material was selected as 1.7 g/cm^3 to be consistent with the conditions expected in the field. A friction angle of 47.6° was obtained from consolidated drained triaxial tests (ASTM D7181-11) conducted in this study to characterize this backfill material.

2.3. Laboratory evaluation to compare EPC Models A and B

A 0.2 m^3 metal drum with an average diameter of 0.6 m was used to conduct the tests to compare the two different EPC models. Figure 1b presents a photo of the aggregate and drum used. A smooth metal plate was installed at the bottom of the drum and a 20 mm HDPE geomembrane lining was placed inside the drum (Figure 1c) to create a uniform surface along the side. The geomembrane was covered with a satin fabric to reduce friction between the aggregate and sidewalls of the drum (Figure 1d). The two EPC models were placed individually at the bottom center of the drum and were loaded in layers with AASHTO No. 8 aggregate up to a thickness of 0.3 m. To create a well-leveled surface, 2000 g of poorly graded sand (SP) were placed beneath the EPCs prior to placement inside the drum and the surrounding area was filled with aggregate (Figure 1d). Before aggregate was placed over the EPCs, Model A was covered with 2500 g of play sand, creating a buffer between the AASHTO No. 8 aggregate and the thin circular plate to minimize the effects of point loading. No sand was placed on top of Model B, as its thicker plates were designed by the manufacturer to reduce the effects of point loading.

To evaluate the responses of the Model A and Model B EPCs to the applied load, a 0.3 m-thick lift of AASHTO No. 8 aggregate weighing approximately 82 kg was placed in the drum in eight layers. The first seven layers were placed, each of which contained a mass of 10 kg, followed by placement of the last layer, which contained 12 kg. Pressure readings were obtained for each layer during loading using the manufacturer calibrations, and results obtained from these tests are presented in Figure 2. The estimated pressure values in Figure 2 were calculated using the density of the aggregate and the thickness of each layer after placement of the aggregate. The response obtained from both EPCs was found to increase linearly, with an increase in applied load exhibiting a similar trend and comparable pressure magnitude. This response confirmed that both EPC models were suitable to obtain

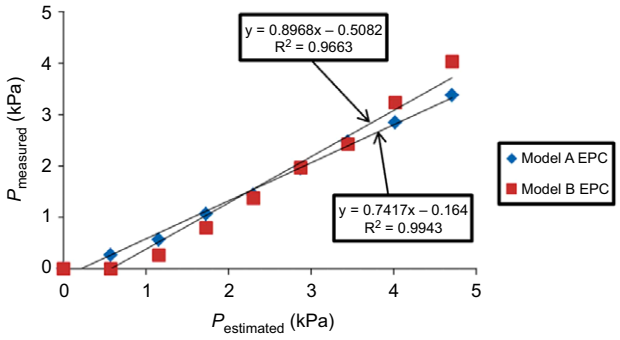

Figure 2. Comparison of calculated (estimated) and measured stress values obtained from two different EPCs evaluated in this study

pressure readings in the field with this particular aggregate. It should be noted that results based on the manufacturer's calibration value did not accurately predict the stress levels. The laboratory measurements were therefore used to recalibrate the pressure gages, emphasizing the importance of performing calibration tests with the actual soil to be used. Model A was ultimately selected due to the better result in terms of correlation (R^2 value) and the difference in cost between the two models. To be consistent with the laboratory evaluation, Model A EPCs were installed in the field using the same type and quantity of sand on top of the instruments.

3. DESIGN OF FIELD INSTRUMENTATION AND IMPLEMENTATION PLAN

The GRS-IBS constructed for this study is located in Harrisonburg, Virginia. The geotechnical investigation carried out at the site showed the geology at the footprint of the abutments to be primarily exposed limestone with pockets of clay. The thicker clay strata were determined to be 2.75 m and classified as high plasticity clay (CH) (ASTM D2487-18). The liquid limit (LL) of the clay was established as 72 and plasticity index (PI) as 45. Overall, the majority of the foundation of both abutments rested directly on bedrock.

The foundation of the structure (referred to herein as reinforced soil foundation (RSF)) was constructed with a typical road base material that corresponded to the classification VDOT 21B aggregate and a woven geotextile with a tensile strength of 70 kN/m. The geotextile was wrapped around the aggregate and an additional geotextile was placed in the middle of the RSF. The overall thickness of the RSF was 0.7 m. The construction procedure followed for the RSF adhered strictly to FHWA guidelines (Adams *et al.* 2011).

The GRS abutment constructed over the top of the RSF was completed using AASHTO No.8 aggregate and the same geotextile used in the RSF. The vertical spacing between geotextile reinforcements was 0.2 m in the primary reinforcement zone and 0.1 m in the bearing bed zone (Figure 3). For the facing of the structure, solid concrete masonry unit (CMU) blocks were used for the

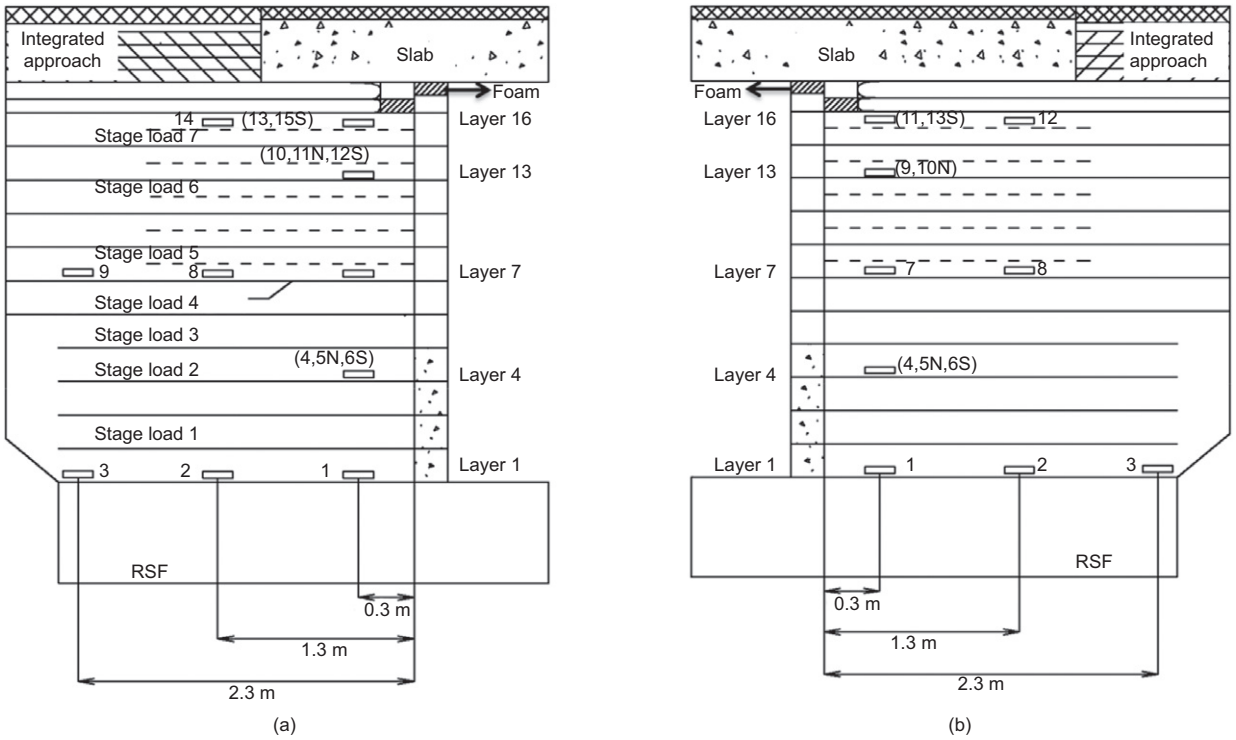

Figure 3. Locations of EPCs: (a) in Abutment A; and (b) in Abutment B. *Notes*: The rectangles depict the locations of the installed EPCs. The hatched rectangles above layer 16 represent the foam placed in between the concrete masonry blocks. N and S stand for the instruments placed along the north and south sides of the abutment along the longitudinal direction to the facing. The dashed lines represent the secondary reinforcements within the bearing bed zone. RSF stands for reinforced soil foundation

first four layers from the bottom and split face CMU blocks were used for the remaining layers, per FHWA guidelines (Adams *et al*. 2011). Both abutments measured 2.2 m in height.

The bridge (superstructure) that rested over the abutments had a span of 3.65 m and a width of 8.5 m. The superstructure was constructed using seven pre-cast concrete segments connected with a steel rod to form a solid slab. The length of the beam seat (the zone that rests directly over the abutment) was different on both sides. The beam seat on the Abutment A side was 0.6 m and 1.2 m on the Abutment B side (Figure 4c). The integrated approach to the bridge involved the same backfill and geotextile reinforcement used to construct the RSF.

The instrumentation plan entailed installation of EPCs in both abutments (i.e. the focus of this paper). In addition, contact pressure cells were installed on the facing units, strain gages and extensometers were installed on the geosynthetics, and survey monitoring points were placed on the facing units as detailed in NCHRP 24-41 (Zornberg *et al*. 2018, 2019). Abutments A and B had 15 and 13 EPCs installed, respectively. The reason for installing more EPCs on abutment A was to generate more data from the stage loading. Additionally, one EPC was placed on a bed of number 8 aggregate inside a box adjacent to Abutment A (not part of the abutment). All EPCs were installed at five different layers within each abutment (layers 1, 4, 7, 13, and 16) (Figure 3). In Abutment A, EPCs were installed in layers 1 and 7, perpendicular to the facing (longitudinally) at 0.3, 1.3, and 2.3 m (only in layers 1 and 7) away from the facing (Figures 3a and 4a). This layout was selected to capture the changes in pressure distribution at points away from the facing blocks and superstructure. In layers 4 and 13, EPCs were installed parallel to the facing of the abutment, with the middle of the instrument resting 0.3 m away from the facing (Figures 3a and 4a). This layout was selected to capture the pressure behind the setback of the superstructure and underneath the beam seat (the zone where the superstructure (slab) rests directly on the abutment). In layer 16, two EPCs were placed parallel to and 0.3 m away from the facing and one EPC was placed perpendicular to and 1.3 m away from the facing. A very similar layout was followed for Abutment B, except in layers 7 and 13, in which only two EPCs were installed in each layer, rather than three as in Abutment A (Figure 3).

The instrumentation layout was designed to include instruments within both primary reinforcement and bearing bed zones, and to obtain data from the north, middle, and south sides of each abutment. The distance from the bottom of the superstructure (the top of the abutment) to the EPCs located in layers 1, 4, 7, 13 and 16 were 2.2, 1.6, 1.0, 0.4 and 0.1 m, respectively. During construction, Abutment A was loaded with Jersey barriers to simulate staged loading. The location of each applied staged load is shown in Figure 3a. In total, there were seven staged loadings, four of which involved the use of eight Jersey barriers and three of which involved the use of a single Jersey barrier. Four staged loadings were applied on the primary reinforcement zone and three staged loadings were applied on the bearing bed zone. Figure 5

Figure 4. Details of the GRS-IBS constructed: (a) installation of EPCs; (b) placement of geotextile reinforcements; (c) placement of bridge slab; and (d) gap between the top of reinforced aggregate and bottom of bridge slab. *Notes*: Figure 4a shows the placement of EPCs at different layers, placed both perpendicular to and parallel with the facing blocks. Figure 4b shows the placement of shorter and longer geotextile reinforcements. These reinforcements are depicted in Figure 3 with dashed lines. Figure 4c shows the differences in beam seat in abutments A and B

Figure 5. Placement of Jersey barriers along the facing of Abutment A to load the structure in stages: (a) single barrier; and (b) multiple barriers. *Note*: Locations of stage loading in different layers have been depicted in Figure 3a

shows the application of staged loadings on the geotextile reinforcement. The bottom of the front Jersey barrier was located 0.2 m from the back of the CMU facing blocks. The Jersey barrier configurations within the abutment profile along with the EPC locations were selected primarily to evaluate the difference in pressure distribution within the primary (single reinforcement) and bearing bed (double reinforcement within the same vertical spacing as in the primary reinforcement) zones.

All EPCs were installed following an approach similar to that followed in the laboratory tests, in which sand was placed below and on top of each cell prior to placement of the backfill aggregate. As the laboratory evaluation confirmed, this approach enhanced the uniformity of the

contact pressure after placement of the granular backfill. Furthermore, this approach was previously recommended to minimize concerns of backfill arching that result in reduced stress measurements (Yang *et al*. 2017; Budge *et al*. 2014).

Figure 4b shows the construction of both abutments with the backfill and geotextile. This specific stage in construction is referred to herein as self-weight condition. Figure 4c shows the placement of the slab. Construction of two beam seats with different lengths facilitated an assessment of the effect of beam seat width on the vertical stress distribution within the abutment. Figure 4d reveals that following placement on top of the reinforced aggregate, some slab segments did not end up making full contact with the aggregate. The gap between the slab and top of the reinforced backfill was observed from slab segments placed in the north and south sides of abutment A and middle and north sides of abutment B. This condition was carefully taken into account in the evaluation of field instrumentation data for this study.

4. EVALUATION AND ASSESSMENT OF FIELD INSTRUMENTATION DATA

4.1. Data generated during construction (short-term behavior)

The purpose of obtaining measurements during construction was to

(1) confirm the validity of the EPC calibrations used in this study
(2) evaluate the stress distribution within backfill reinforced using different vertical reinforcement spacings (i.e. 0.2 m spacing below bridge seat and 0.1 m spacing within the bridge seat)
(3) understand whether the staged loading had an effect on the overall vertical stress conditions within the abutment
(4) evaluate the effects of different beam seat dimensions on the stress distribution within the GRS.

4.1.1. *Vertical stress measurements from EPCs due to self-weight*

This evaluation was conducted to confirm that the pressure values obtained from the EPCs were consistent with the theoretically calculated values for a specific depth. Stresses measured at the first (bottom) layer of both abutments have been presented in Figure 6 as representative examples for this evaluation. Figure 6 depicts the changes in pressure values from three EPCs located in each abutment. The pressure values increased over time as the layers of the GRS were constructed. At the end of construction and before the placement of the slab, the vertical stresses measured by all EPCs in both abutments reached a value close to 36 kPa. Considering these EPCs were located 2.2 m below the top of the abutment and the aggregate used in construction had a unit weight of 16.5 kN/m^3, the values measured by the EPCs were in good agreement with the calculated overburden stress of 36.3 kN/m^2. This comparison confirms the validity of the instruments' calibrations and their accuracy to estimate stresses purely based on self-weight of the backfill material.

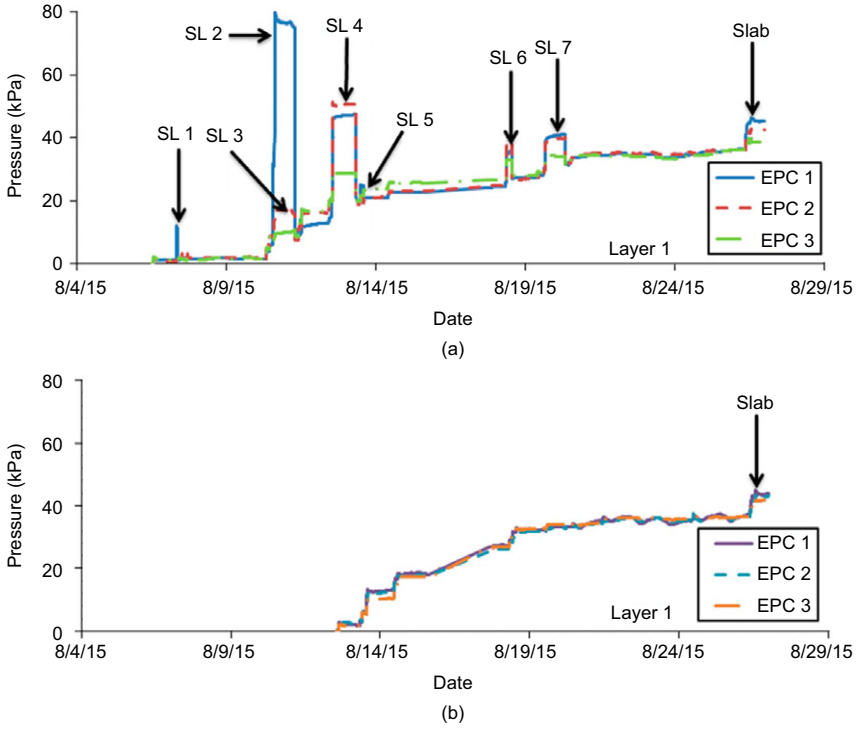

Figure 6. Vertical stresses recorded at layer 1 during construction: (a) Abutment A; and (b) Abutment B. *Notes*: Peaks shown in the figure represent the response of EPCs values due to staged loading. Only Abutment A was loaded in stages. Definition of layer 1 is shown in Figure 3

The peak values shown in Figure 6a refer to the data obtained during staged loading, which is discussed in the subsequent section. However, the pressures recorded by EPCs during staged loading increased, as the results in Figure 6a make evident. After the removal of the load, pressures decreased, but to a level slightly higher than the pressures recorded before staged loading. While these changes were observed, the overall stress levels reached in Abutment A were approximately the same as those reached in Abutment B when construction of the abutments was completed (comparison of Figures 6a and 6b). This indicates that the staged loading implemented in this study generated additional vertical stresses in Abutment A during its construction, but they were ultimately overcome by the actual design load.

The vertical stresses recorded in both abutments by all EPCs at the same depth (i.e. EPCs 1, 2, and 3 as shown in Figure 6) provided similar values, regardless of the EPC's location within the abutment. In both abutments, EPC 1 was right underneath the zone where the slab was placed (close to the GRS facing), with the other EPCs located closer to the integrated approach (away from the GRS facing). This uniform stress distribution is believed to be a consequence of very small (i.e. less than 5 mm) facing deformations. In other studies where deformations along the facing were significant (e.g. up to 76 mm), the vertical stresses recorded close to and away from the GRS facing differed from one other (Desai and El-Hoseiny 2005; Jiang *et al*. 2015).

4.1.2. *Effect of vertical reinforcement spacing on stress distribution as observed from Abutment A – staged loading*

Staged loading was conducted during the construction of Abutment A to evaluate the effects of differences in vertical spacing (S_v) between reinforcements on the stresses recorded within the GRS. In the primary reinforcement zone, S_v was 0.2 m, and in the bearing bed zone, S_v was 0.1 m (essentially double the reinforced zone). Therefore, a comparison of the vertical stress distribution in each of these zones could be used to evaluate the effects of reinforcement spacing.

Staged loading was carried out by placing multiple Jersey barriers over the GRS at different heights. Due to time constraints, some layers were loaded with only a single Jersey barrier, as placement of multiple Jersey barriers required more time. The loading phase ranged from 30 min to 24 h due to scheduling constraints during construction.

The Jersey barrier used in the staged loadings was 0.6 m wide and 3.6 m long and the magnitude of the pressure from one barrier was approximately 11 kPa. In the case of eight Jersey barrier applications, three were placed directly on the geotextile layer and the remaining five were stacked on top of the three. However, the second of the three lower barriers was not in contact with the top five barriers due to the geometric shape of the Jersey barrier (Figure 5b). Therefore, the calculation of the load was conducted based on the first and third barriers of the 3 lower barriers to carry the load from the top five barriers. This resulted in a total load of 89 kPa, where the first and third barrier each applied approximately 39 kPa and the middle barrier was applying 11 kPa. Figure 7a displays the response of EPCs 1 and 7 when both instruments were loaded with a single Jersey barrier that was located 0.8 m above the EPCs. EPC 1 was loaded as part of stage load 3 and located within the zone where $S_v = 0.2$ m. EPC 7 was loaded as part of stage load 7 and located within the zone where $S_v = 0.1$ m. Although stage load 7 included eight Jersey barriers, the comparison was made when only the first Jersey barrier was placed on the GRS. The results show that the stress measured by EPC 1 was higher than EPC 7, indicating that the stress values within the primary reinforcement zone (where the spacing between the reinforcements are larger) were higher than the ones in the bearing bed zone.

Figure 7b presents the responses of EPCs 1, 2 and 3 to stage load 4 (in the zone where $S_v = 0.2$ m) and EPCs 7, 8 and 9 to stage load 7 (in the zone where $S_v = 0.1$ m). In this comparison, both staged loads were conducted with multiple Jersey barriers (39 kPa), but the vertical distance between the location of the applied load and the instruments was 1.2 m and 0.8 m in stage load 4 and 7, respectively. The results show that reduced stresses were measured by EPCs 7, 8 and 9, even though these instruments were located a shorter vertical distance from the applied load as compared to EPCs 1, 2 and 3. The stress measured by EPC 3 was less than the stresses recorded by EPCs 1 and 2, and the stress measured by EPC 9 was less than the stresses measured by EPCs 7 and 8 because EPCs 3 and 9 were horizontally farther away from the location of the applied load (Figure 7b). Nonetheless, the stress measured by EPC 3 was higher than that measured by EPC 9. These observations indicate a reduction in the stress distribution in the zone where reinforcements were vertically closer to each other (i.e. within the bearing bed zone).

The consistent trends observed in Figure 7 (with both single and multiple Jersey barriers) demonstrate that closely spaced reinforcements contribute to reduced vertical stresses in the GRS bearing bed zone. In single Jersey barrier loading, the magnitude of stress was reduced 1.8 times and in multiple Jersey barrier loading, the magnitude of stress was reduced 2.7 to 5.4 times. Moreover, this indicates that the effect of closely spaced reinforcements becomes more prominent with an increase in applied loads. Overall, the results obtained from the staged loadings reveal that a decrease in reinforcement spacing (increased number of reinforcements) leads to reduced vertical stresses in the GRS mass.

4.1.3. *Effect of beam seat width on stress distribution – slab loading*

The purpose of this evaluation was to compare the differences in stress distribution within the GRS when one abutment had a beam seat width of 0.6 m (Abutment A), which is the minimum width required considering the length of the bridge span, and the other abutment had a beam seat width of 1.2 m (Abutment B, twice the width of Abutment A). Although both abutments were loaded with the same slab, the magnitude of surcharge

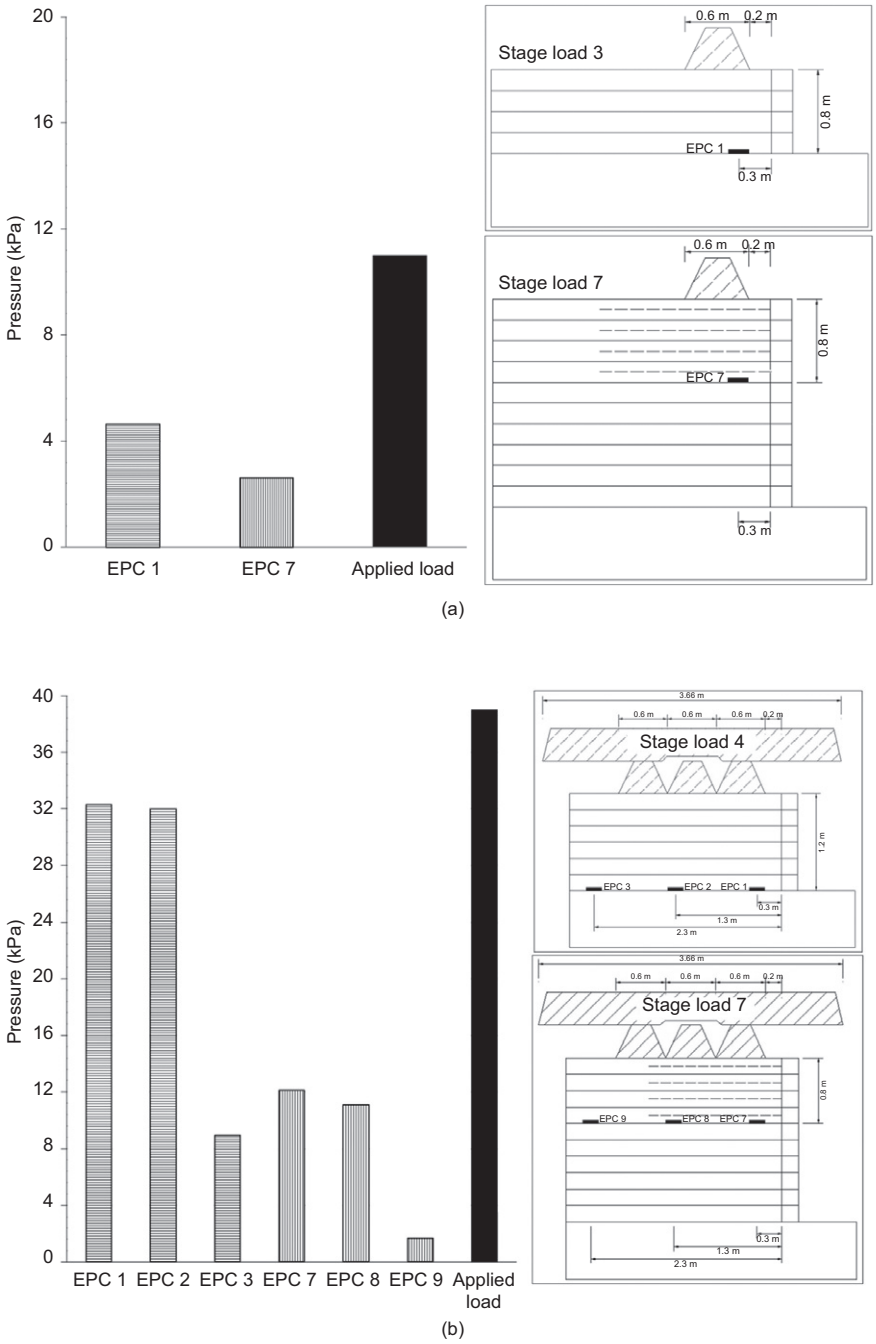

Figure 7. Comparison of vertical stresses measured in the PR and BB zones in response to staged loading: (a) stresses measured from single Jersey barrier; and (b) stresses measured from multiple Jersey barriers. *Notes*: The term primary reinforcement (PR) zone represents layers 1–7 shown in Figure 3. The term bearing bed (BB) zone represents layers 8 and above shown in Figure 3, where the structure consists of reinforcements placed 0.1 m apart

loads in Abutments A and B were estimated to be 42 and 21 kPa, respectively.

Figure 8 shows the vertical stress distribution profiles developed in each abutment based on the data obtained from EPCs located in the middle, north and south sides of each abutment. The comparison shows that in both abutments, the applied load was distributed throughout the GRS and the magnitude of measured pressures decreased with depth. Although the applied load was the same throughout each abutment, the EPCs installed in the middle, north and south sides provided different values. This discrepancy is believed to be due to a gap that may have developed between some of the slab segments and the top of the reinforced aggregate within the abutment, as can be seen in Figure 4d. The presence of a gap has also been noted by Zheng *et al.* (2019) during the research conducted on physical model GRS abutments. The effect of the gap in the field was more pronounced on EPCs located at a depth of 0.1 m, where, contrary to expectations, very low stresses were measured due to the slab load. Consequently, the stresses measured at a depth of 0.1 m are not included in Figure 8. When comparing the data from the EPCs located at the middle of each abutment, irrespective of the magnitude of the slab load,

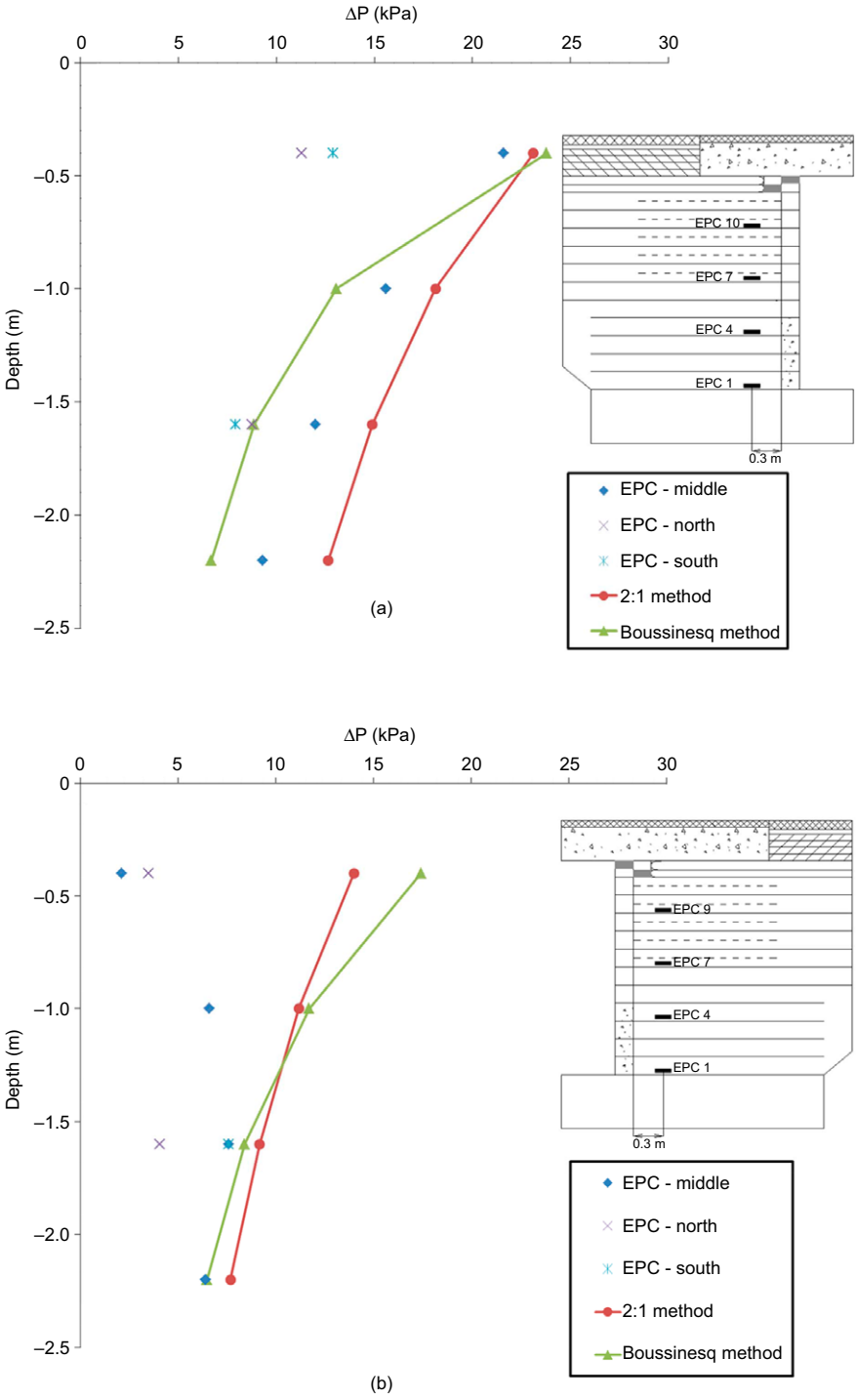

Figure 8. Comparison of measured and calculated vertical stress distributions due to bridge slab load (Δ*P*): (a) Abutment A; and (b) Abutment B. *Notes*: Values shown with EPC labels were obtained from field measurements along the middle, north and south sides of the facing. Stress distributions were calculated using the approximate 2 : 1 method and the Boussinesq method. Δ*P* represents the values that were generated after the placement of the bridge slab (it excludes the stresses generated by the self-weight of the abutment)

an approximately 1/4 reduction in the applied load was observed (i.e. 42 kPa reduced to 10 kPa and 21 kPa reduced to 5 kPa). This indicates that the mechanism of vertical stress distribution does not change based on changes in the beam seat width, but that the beam seat dimensions have of course a significant effect on the applied load. This information could be used to adjust the beam seat to apply lower loads on the GRS or to adjust the height of the bearing bed (double reinforced zone), as a wider beam seat would induce lower pressures on the GRS.

4.2. Data generated after construction (long-term behavior)

An assessment was conducted of the long-term performance of the GRS-IBS in relation to vertical stresses and stress distribution by evaluating the effects of

post-construction transitional loadings on the superstructure and stresses recorded by the EPCs over time.

4.2.1. *Effect of seasonal variations on vertical stresses*

A laboratory test conducted to study the suitability of the EPCs to measure stresses in various types of soils showed that the instruments generated stresses within ±15% of the expected soil stresses (GEOKON 2018). To assess the sensitivity to seasonal changes of the EPCs used in this study, an additional evaluation was carried out using an EPC installed outside the GRS abutment. One EPC was placed at the bottom of a wooden box (0.6 m wide and 0.5 m high) and filled with 0.18 m of AASHTO No. 8 aggregate (Figure 9). Data collected for approximately 2 years from this EPC is given in Figure 10, along with the corresponding average monthly temperature and cumulative monthly precipitation data obtained from a nearby weather station. The stress measured by the EPC was corrected for changes in temperature with time using Equation 8. Figure 10b shows the temperature measured by the thermistor embedded inside the EPC and the ambient temperature measured from the weather station. As displayed in Figure 10b, the temperatures measured by the two sources showed similar trends over time, with lower temperatures during fall and winter seasons and higher temperatures during spring and summer seasons. Figure 10a presents a comparison of the measured stress (uncorrected and corrected) and the stress calculated theoretically using the unit weight of the aggregate and thickness of the fill. The uncorrected stress data revealed that the earth pressure cell was sensitive to temperature changes with seasonal variations. The stresses in colder seasons were lower than the stresses in warmer seasons. The magnitude of the uncorrected stress was close to the calculated stress when the EPC was loaded with the aggregate. However, as the temperature changed with time, the magnitude of the measured stress was less than the calculated stress. When a correction to the temperature was applied, the magnitude of stress became more similar to the theoretically calculated stress. At times when higher precipitation (Figure 10c) was observed, the magnitudes of measured stresses were also higher due to the added water weight. However, the increase in stress due to precipitation dissipated within a short period because AASHTO No. 8 aggregate is a free draining material and water was able to drain through a hole made in the bottom of the box. The small increase in stress during

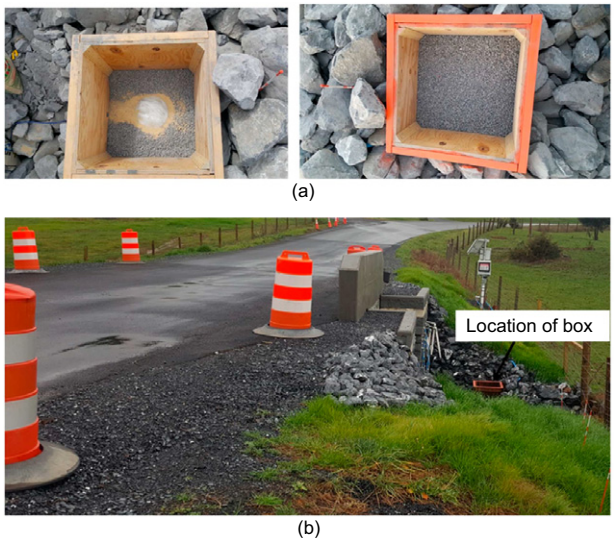

Figure 9. EPC 16 placed inside a wooden box outside the GRS-IBS: (a) placement of EPC before being covered with aggregate; and (b) location of the box

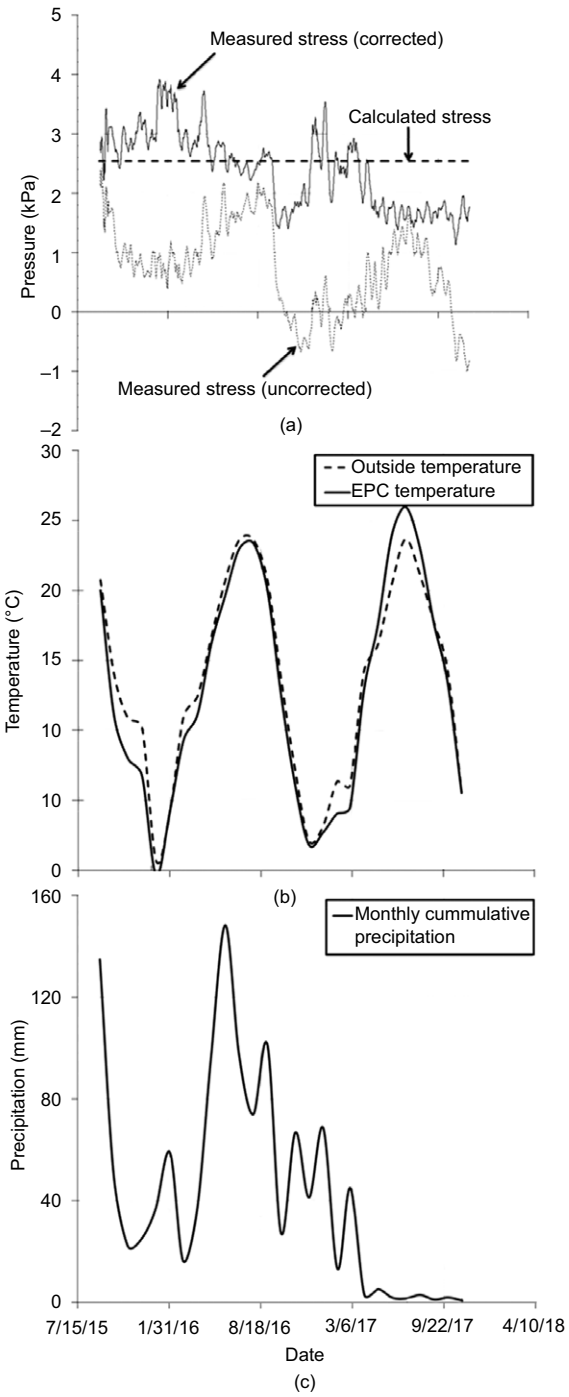

Figure 10. (a): Fluctuation of vertical stress values from EPC inside wooden box; (b) average recorded monthly temperatures; and (c) average recorded monthly cumulative precipitation. *Note*: Each value shown in Figure 12c represents the total cumulative precipitation for a given month

winter seasons could have been caused by an accumulation of snow over the gravel in the box that was observed during a regular post-construction site visit in wintertime (e.g. December 2015 to January 2016). Altogether, these seasonal effects appear to have resulted in an approximately 50% change in measured stresses (i.e. average readings of 2.5 kPa), despite the corrections applied to pressure values based on temperature fluctuations. Nonetheless, a comparison of the subsequent incremental readings revealed that the changes in pressure with time were within the instrument's range of accuracy.

4.2.2. *Effect of transitional loading on vertical stresses in GRS abutments – truck loading*

This evaluation was conducted to observe the vertical stress distribution within the GRS when the superstructure was loaded with a truck and to note any changes in the measured vertical stress values when the truck load was applied at different times of year (seasonal differences). To complete this evaluation, a truck was parked over the bridge superstructure at four different times throughout the year, beginning in September (response immediately after construction), then in December (response during winter season), followed by March (response during spring season) and lastly November (response during fall season). The truck selected for loading was a single axle truck (AASHTO H-15 category) with a length that allowed all tires to rest directly on top of the slab. Figure 11 shows the configuration of the parked truck over the slab. During loading, the truck was parked in 4-h intervals on each side of the traffic lanes (north- and southbound) due to traffic control limitations. The truck was filled with aggregate and had a gross weight of 150 kN. Based on the AASHTO standard, the load from the front axle was 1/3 of the load from the rear axle, in which the front axle carries 50 kN and the rear axle carries 100 kN of the gross weight. Since the truck was parked for 4 h in each lane, the surcharge in Abutments A and B was calculated using the gross weight of the truck and the area over the beam seat. The surcharge from the truckload was approximately 14 kPa in Abutment A and 7 kPa in Abutment B. The surcharge in Abutment A was twice that of the surcharge in Abutment B based on the width of the beam seats (i.e. the beam seat width in Abutment A was half the width in Abutment B). The average stresses measured by the EPCs throughout the 8 h of loading (4 h per lane) was considered in the stress distribution evaluation to capture the difference in magnitude of load from the front and rear axles.

Figure 12 shows the additional stress distribution profiles from the truckload in Abutments A and B. As was observed when the slab was placed over the GRS, vertical stresses in Abutment A appeared to be higher than in Abutment B, which confirms that a wider beam seat could effectively reduce the vertical stress distribution in a GRS abutment due to imposed superstructure loads. In Abutment A, higher stresses from the September 2015 and March 2016 truck loadings were observed. This increase in stresses could be a result of water infiltration into the abutment during the rainy seasons (Figure 10c), which would support the observations made from the stress data in the box outside the abutment. However, the differences in stress magnitude measured in the four truck loadings was only in the range of 1.5 to 2 kPa in the top sections of Abutment A. At lower elevations, the difference was as small as 0.3 kPa. In Abutment B, the differences in stress magnitude measured in the four truck

Figure 11. Truck loading on the superstructure after construction: (a) side view; (b) front view; and (c) rear view. *Note*: Truck was parked on each lane

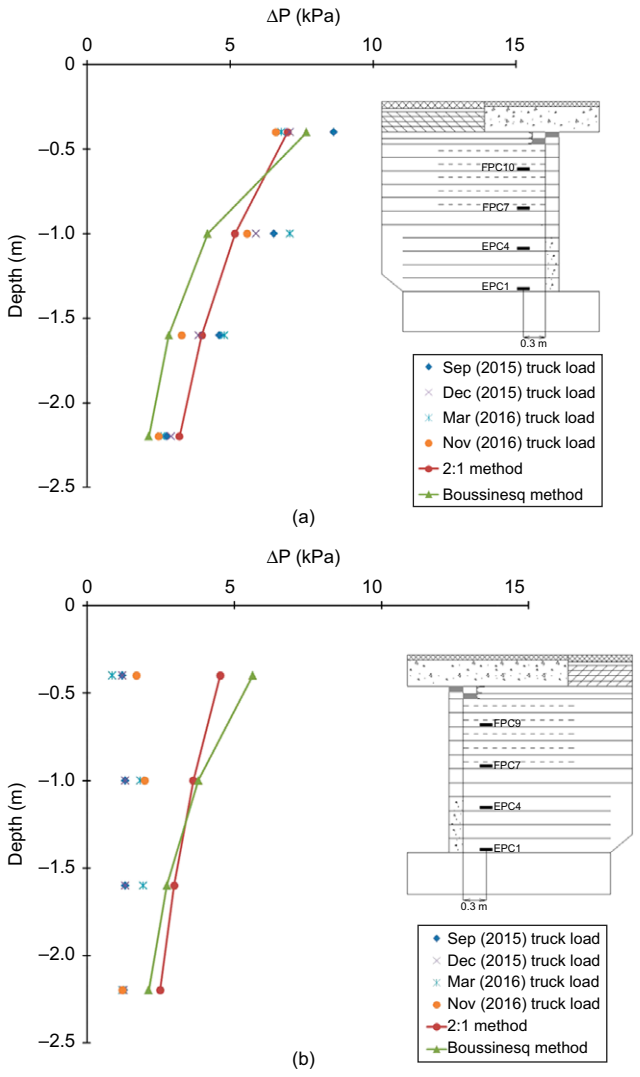

Figure 12. Comparison of measured and calculated vertical stress distributions due to truck loading (Δ*P*): (a) Abutment A; and (b) Abutment B. *Notes*: Values shown with date were obtained from the field measurements from earth pressure cells along the facing. Stress distributions were calculated using the approximate 2 : 1 method and the Boussinesq method. Δ*P* represents the values that were generated after the placement of the truck (it excludes the stresses generated by the self-weight of the abutment and bridge slab)

loadings was in the range of 0.4 to 0.8 kPa. If evaluated in terms of percentages, these differences would range from 15 to 30%. However, when evaluated in terms of magnitude, these differences are well within the instrument's range of accuracy of ±15%. Overall, the vertical stress distribution in the GRS abutment with AASHTO No. 8 aggregate used as backfill material was not significantly influenced by seasonal variations.

5. EVALUATION OF FIELD INSTRUMENTATION DATA FROM OTHER PROJECTS

A comparison was conducted of the vertical stress distribution observed in this study after placement of the slab with observations from two other projects located in Louisiana (another GRS-IBS structure) and Colorado (MSE bridge abutment). The data for the Colorado site was directly available and the data for the Louisiana site was obtained from the published journal article by Saghebfar *et al.* (2016).

The Louisiana field site is located on Route LA 91 close to Vermilion Parish, and consists of a structure with a bridge span of 22 m, abutments 4.3 m in height and a beam seat width measuring 1.5 m. The beam seat width was selected according to the FHWA's design guidelines based on the length of the bridge span. When compared with the GRS-IBS constructed for this study (i.e. the Virginia GRS-IBS), the 1.5 m beam seat for the Louisiana structure would be equivalent to the beam seat of Abutment A. The dead load for the bridge slab is estimated at around 100 kPa. The backfill material used at this site was an open-graded crushed rock with a maximum particle size of 12.7 mm and maximum dry density of 2.1 gm/cm^3. Based on large scale direct shear tests, the friction angle of the aggregate was characterized as 50.9°. A woven geotextile with an ultimate tensile strength of 80 kN/m was used as reinforcement. The vertical reinforcement spacing in the primary reinforcement zone was 0.2 m and 0.1 m in the bearing bed zone. The EPCs used at this site were installed in only one abutment, and placed horizontally, 0.6 m from the facing and at depths of 0.4 and 1 m below the superstructure.

The Colorado field site is located along I-70 over Smith Road and consists of an MSE bridge abutment (without a bearing bed with twice the density of reinforcement) with two multi-span bridges approximately 50 m long and abutments 4.3 m high. The footing of the bridge was placed over the MSE wall and the width of the footing was 2 m. The dead load from the bridge girder in the instrumented section of the abutment was 44.5 kPa. Class I structural backfill was reinforced with a woven geotextile with an ultimate tensile strength of 80 kN/m. The maximum particle size of the aggregate was 12.5 mm with a maximum dry density of 2.2 gm/cm^3. The friction angle was characterized as 51.8°. The reinforcements were vertically spaced 0.1 m apart from each other. The facing element was constructed with a sheet pile to which the reinforcements were not connected. EPCs for vertical stress measurements were placed horizontally, right below the superstructure, at depths of 1.2, 2.7, and 4.3 m from the top of the abutment. All instruments were located 0.3 m from the facing.

The stress distribution in the abutment after placement of the bridge superstructure for the Louisiana and Colorado projects is presented in Figure 13. The stress values shown in Figure 13 only represent the stresses generated due to the superstructure load and thus exclude the stresses generated by the self-weight of the abutment. The results exhibit a trend similar to the GRS-IBS structure constructed for this study, in which the slab load was distributed through the abutment all the way to the foundation level. For instance, in the Virginia and Louisiana GRS-IBS, the stresses measured at a depth of 1 m were 62 and 80% of the superstructure load, respectively. At the Colorado site, the stress measured at a depth

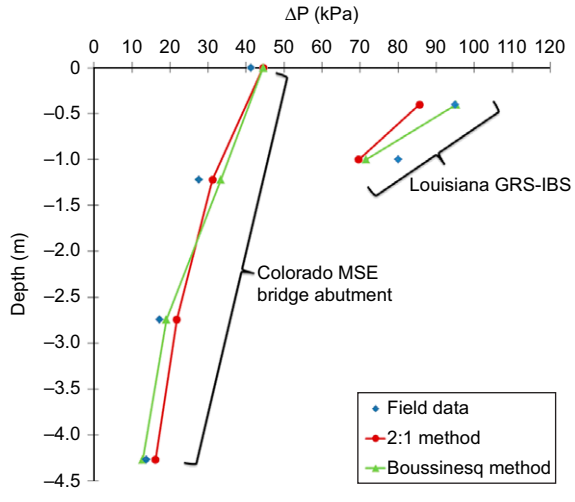

Figure 13. Comparison of measured and calculated vertical stress distributions due to slab loading (Δ*P*) in Louisiana GRS-IBS and Colorado MSE bridge abutment. *Notes*: Field data refers to stresses measured from EPCs installed 0.6 m from the facing in Louisiana GRS-IBS and 0.3 m from the facing in Colorado MSE bridge abutment. Stress distributions were calculated using the approximate 2 : 1 method and the Boussinesq method. Δ*P* represents the values that were generated after the placement of the slab (it excludes the stresses generated by the self-weight of the abutment)

of 1.2 m was 60% of the superstructure load. A comparison of the three sites indicates that the loads from the superstructure transferred at the Virginia and Colorado sites, regardless of the bridge span lengths and height of the abutment, even though the Colorado site did not have an EPC at the bottom of the GRS abutment to confirm this claim. However, the EPC located below the reinforced soil foundation supported this observation. And in all cases, the stress distribution due to superstructure loads reduced with depth (not a uniform distribution).

6. COMPARISON OF THEORETICAL VERTICAL STRESS DISTRIBUTIONS TO THE FIELD MEASUREMENTS

All data obtained from field measurements were compared to the theoretical stress distributions calculated based on AASHTO's 2 : 1 method and the Boussinesq method, as provided in Equations 1–5.

Figures 8 and 12 present a comparison of field measurements based on the slab and truck loads, respectively, with the estimated stress distributions from the Virginia GRS-IBS. In Figure 8, the calculations show that the difference in stress magnitudes as a result of different beam seat widths is between the order of 1.5 to 2 close to the top of the abutment. As expected, these differences decreased with depth as the magnitude of distributed stress decreased at a higher depth. The stress distribution methods considered in this study show similar stress distribution trends. However, when comparing the magnitudes of stress with the field data, the Boussinesq method appears to provide stress magnitudes closer to the field data than the approximate 2 : 1 method. At a higher depth, the stress distribution from the field was reasonably in agreement with the stress distribution methods. However, the stresses measured at the top sections of abutments in the field were lower than the stresses calculated using the two methods. As previously discussed, the lower pressure magnitudes are believed to have been caused by the gap beneath the slab segments and top of the reinforced aggregate. In all cases, the approximate 2 : 1 method appears to be over predicting the field measurements by about 10 to 20%. In the case of stress distribution due to truck loading (Figure 12), the stress distribution profiles obtained from field measurements were observed to be in agreement with the stress distributions predicted by theoretical methods. As in the case of the slab load, the gap beneath the slab segments and top of the reinforced aggregate affected the stresses measured in the top sections of the abutments in the case of the truck loading. Based on the results in Figures 8 and 12, the observations indicated that the Boussinesq method used in the design of GRS-IBS provides a better prediction of the vertical stress distribution due to superstructure loads.

Figure 13 shows a comparison of stress distributions from field measurements in the Louisiana and Colorado sites with the stress distributions predicted by the approximate 2 : 1 and the Boussinesq methods. The vertical stress distribution from the Louisiana site shows that the stresses measured by the EPCs within the bearing bed zone were comparable with the calculated stresses. The stresses measured in the field from the Colorado site were lower than the stresses predicted by the Boussinesq method by 10 to 20% in upper portions of the abutment. However, the stresses measured at lower elevations were in reasonable agreement with the stresses estimated using the Boussinesq method. The approximate 2 : 1 method provided the same stress levels as the Boussinesq method in upper and lower portions of the abutment.

A comparison of the results in Figures 8 and 12 indicate that the vertical stress distribution from the field followed a similar trend as the stress distribution predicted using theoretical methods. Apart from the stresses measured at a depth of 1 m at the Louisiana site, the stresses measured in the field were in general less than the theoretically estimated stresses. The Boussinesq method in the design of GRS-IBS provided stress values more comparable to stresses measured in the field than the approximate 2 : 1 method used in the design of MSE structures. The approximate 2 : 1 method appeared to overestimate stresses by up to 20% in structures reinforced at 0.1 m and 0.2 m spacing. This indicates that for closely and widely spaced structures, the Boussinesq method provides a better analytical solution than the approximate 2 : 1 method.

7. CONCLUSIONS AND PRACTICAL IMPLICATIONS

This study presented an assessment of vertical stress distribution mechanisms in GRS-IBS structures by

evaluating instrumentation data obtained from EPCs installed within actual abutments (not test sites) in the field. The effect of staged loading on the compaction of reinforced soil, vertical reinforcement spacing, beam seat width, and seasonal variations on vertical stresses and stress distribution mechanisms were evaluated. The stress distribution obtained from the field was compared with the theoretical approaches used in the design of GRS and MSE structures. The findings and conclusions from this study are presented below.

(1) The vibrating wire EPCs used in this study were found to be reliable in their vertical stress measurements of GRS structures. Placing sand below and on top of the instrument was found to enhance uniform contact loading from backfill material and mitigate potential arching effects to generate reliable data. This also facilitated utilizing EPCs with thinner plates to measure stresses in granular soils rather than EPCs with thicker plates.
(2) Preloading coarse aggregate backfill with Jersey barriers as part of staged loading did not induce any additional stresses that affected the overall stress distribution within the GRS. The stresses observed due to self-weight of the backfill in the GRS abutments close to the facing were the same as the stresses farther away from the facing. This may have occurred as a result of the very small vertical and lateral deformations of the facing, which did not affect the interaction of the facing with the backfill and geotextile and the vertical stresses behind the facing. These observations are consistent with observations from a Louisiana GRS-IBS (Saghebfar *et al*. 2016). However, these observations differ from observations by Desai and El-Hoseiny (2005) and Jiang *et al*. (2015), although the reinforcements in those studies were connected to the facing mechanically (rather than the typical frictional connection in GRS-IBS) and the lateral deformations observed were high.
(3) The results from staged loading revealed that the response of the EPCs in the primary reinforcement zone ($S_v = 0.2$ m) was higher than the EPCs in the bearing bed zone ($S_v = 0.1$ m). In single Jersey barrier loadings, the stress magnitudes were reduced 1.8 times and in multiple Jersey barrier loadings, the stress magnitudes were reduced 2.7 to 5.4 times. This trend demonstrates that closely spaced reinforcements contribute to a reduction in vertical stresses in the bearing bed zone.
(4) The width of the beam seat affects the stress distribution within the GRS abutment. A wider beam seat was shown to effectively reduce the stress distribution in the structure as a result of superstructure and transitional loads. Adjusting the beam seat width is an approach that can be used to lower the magnitude of the load from the superstructure on the GRS-IBS and induce lower pressures on the GRS. However, it should be noted that even with a wider beam seat, the slab load transferred all the way to the bottom of the GRS-IBS. Where ground conditions are soft, depending on the transferred stresses, the construction of a reinforced soil foundation may become an important design requirement, as prescribed by the FHWA.
(5) The approximate 2 : 1 method in the design of MSE structures (Berg *et al*. 2009) and the Boussinesq method in the design of GRS-IBS (Adams *et al*. 2011) showed similar stress distribution trends when compared to stress distribution obtained from the field monitored GRS-IBS in Virginia and Louisiana and the MSE bridge abutment in Colorado. However, the Boussinesq method appears to provide values more comparable to the field data than the approximate 2 : 1 method. The approximate 2 : 1 method appears to be over predicting the field measurements by up to 20% in structures reinforced at 0.1 and 0.2 m spacing. The stresses measured in top sections of the GRS-IBS were lower than the theoretically estimated stresses as a result of the presence of the bearing bed. Overall, the Boussinesq method provides a better stress distribution than the approximate 2 : 1 method, although to be conservative the designers may choose to utilize the approximate 2 : 1 method over the Boussinesq method.
(6) The long-term vertical stress measured in the box outside the abutment showed that the EPCs were sensitive to changes in temperature over time, although a correction can be applied to minimize this sensitivity. EPCs are also sensitive to the effects of seasonal changes that actually influence the vertical stress such as rain and snow accumulation as well as very dry periods during which all the moisture within the reinforced fill has evaporated. These effects led to higher vertical stresses in the GRS abutment in spring and summer seasons. This observation was also consistent with stress data from an EPC installed in a box outside the abutment. Overall, when comparing the actual differences in magnitudes of pressure measurements, it can be asserted that the vertical stresses and stress distribution in the GRS abutments constructed with AASHTO No. 8 aggregate backfill were not significantly influenced by seasonal variations. This confirms the suitability of this material for use in the construction of GRS abutments.

ACKNOWLEDGMENTS

This research was funded by the National Cooperative Highway Research Program (NCHRP) and Virginia Department of Transportation (VDOT). VDOT's Staunton District also designed and constructed the GRS-IBS cited in this research. The authors would like to thank researchers at the Virginia Center for Transportation Innovation and Research (VCTIR) and VDOT, especially M. Brown, R. Pearce, C. Weaver,

J. Eulogio, I. Kim, J. Calhoun and J. Uhl. We would like to thank R. Drefus at Geocomp for his support in field instrumentation data collection systems and M. Vessely at Shannon and Wilson for providing access to the Colorado MSE bridge abutment instrumentation data. We are also grateful to A. Abbaspour, S. Ullah, A. Morsy and Y. Jiang for their generous help in the field while they were graduate students.

NOTATION

Basic SI units are given in parentheses.

b	width of the footing (m)
D	effective width of the applied load at a given depth (m)
d	distance from the facing to the center of footing width (m)
e	eccentricity of footing load (m)
G	calibration factor (dimensionless)
K	thermal factor (dimensionless)
L	length of footing (m)
P	pressure (N/m^2)
Q	load on isolated footing (N)
q	surcharge pressure (N/m^2)
R_0	initial digits (frequency) reading (Hz)
R_1	current digits (frequency) reading (Hz)
R^2	coefficient of determination
S_v	vertical reinforcement spacing (m)
T_0	initial temperature reading (C)
T_1	current temperature reading (C)
Z	depth of stress point below footing (m)
Z_1	depth at which the effective width intersects the back of the wall facing (m)
α, β	inclination angles for stress distribution point of interest (°)
γ_b	unit weight of backfill material (N/m^3)
$\Delta\sigma_v$	distributed vertical stress (N/m^2)

ABBREVIATIONS

AASHTO	American Association of State Highway and Transportation Officials
EPC	Earth pressure cell
FHWA	Federal Highway Administration
GRS	Geosynthetic reinforced soil
GRS-IBS	Geosynthetic reinforced soil-integrated bridge system
IBS	Integrated bridge system
MSE	Mechanically stabilized earth
RSF	Reinforced soil foundation
VDOT	Virginia Department of Transportation

REFERENCES

AASHTO (American Association of State Highway and Transportation Officials) (2016). *LRFD Bridge Design Specifications*, 7th edn, with 2015 and 2016 Interims, American Association of State Highway and Transportation Officials, Washington, DC, USA.

Abu-Hejleh, N., Zornberg, J. G., Elias, V. & Watcharamonthein, J. (2003). Design assessment of the Founders/Meadows GRS abutment structure. *Proceedings of the 82nd Annual Meeting*, Transportation Research Board, Washington, DC, USA (CD-ROM).

Abernathy, C. (2013). *Experimental Projects Construction Report – Geosynthetic Reinforced Soil – Integrated Bridge System (GRS-IBS)*, Report No. MT-12-04. Montana Department of Transportation, MT, USA.

Adams, M. T., Schlatter, W. & Stabile, T. (2007). Geosynthetic reinforced soil integrated abutments at the Bowman Road bridge in Defiance County, Ohio. In *Geosynthetics in Reinforcement and Hydraulic Applications*, Gabr, M. A. & Bowders, J. J., Editors. American Society of Civil Engineers, Reston, VA, USA, Geotechnical Special Publication no. 165, pp. 1–11.

Adams, M. T., Nicks, J. E., Stabile, T., Wu, J. T. H., Schlatter, W. & Hartmann, J. (2011). *Geosynthetic Reinforced Soil Integrated Bridge System, Synthesis Report*, Report No. FHWA-HRT-11-027. Federal Highway Administration, McLean, VA, USA.

Adams, M. T., Nicks, J. E., Stabile, T., Wu, J. T. H., Schlatter, W. & Hartmann, J. (2012). *Geosynthetic Reinforced Soil Integrated Bridge System Interim Implementation Guide*, Report No. FHWA-HRT-11-026. Federal Highway Administration, McLean, VA, USA.

ASTM D2487-18. *Standard Practice for Classification of Soils for Engineering Purposes (Unified Soil Classification System)*. ASTM International, West Conshohocken, PA, USA.

ASTM D7181-11. *Standard Test Method for Consolidated Drained Triaxial Compression Test for Soils*. ASTM International, West Conshohocken, PA, USA.

Berg, R. R., Christopher, B. R. & Samtani, N. C. (2009). *Design and Construction of Mechanically Stabilized Earth Walls and Reinforced Soil Slopes*, FHWA NHI-10-024 Vol I and NHI-10-025 Vol II, U.S. DOTFHWA-NHI-09-083 and FHWA GEC-011. Federal Highway Administration, Washington, DC, USA.

Bloser, S., Shearer, D., Corradini, K. & Scheetz, B. (2012). *Geosynthetically Reinforced Soil-Integrated Bridge Systems (GRS-IBS) Specification Development for PennDOT Publication 447*, Publication No. 447 (10-14). Pennsylvania Department of Transportation, Harrisburg, PA, USA.

Budge, A. S., Dasenbrock, D. D., Mattison, D. J., Bryant, G. K., Grosser, A. T., Adams, M. & Nicks, J. (2014). Instrumentation and early performance of a large grade GRS-IBS wall. In *Geo-Congress 2014 Technical Papers: Geo-Characterization and Modeling for Sustainability*, Abu-Farsakh, M., Yu, X. & Hoyos, L. R., Editors. American Society of Civil Engineers, Reston, VA, USA, Geotechnical Special Publication no. 165, pp. 4213–4227.

Christopher, B. R. (1993). *Deformation Response and Wall Stiffness in Relation to Reinforced Soil Wall Design*, PhD dissertation, Department of Civil Engineering, Purdue University, West Lafayette, IN, USA.

Desai, C. S. & El-Hoseiny, K. E. (2005). Prediction of field behavior of reinforced soil wall using advanced constitutive model. *Journal of Geotechnical and Geoenvironmental Engineering, ASCE*, **131**, No. 6, 729–739.

FHWA (Federal Highway Administration) (2006). *Soils and Foundations – Volume I*, FHWA NHI-06-089, Federal Highway Administration, Washington, DC, USA.

FHWA (2019). *Everyday Counts Initiative (EDC-3), Geosynthetic Reinforced Soil-Integrated Bridge System (GRS-IBS)*, FHWA, McLean, VA, USA. See https://www.fhwa.dot.gov/innovation/everydaycounts/edc-3/grs-ibs.cfm.

GEOKON (2018). *Vibrating Wire Earth Pressure Cells*, Instruction manual, Geokon, Lebanon, NH, USA. https://www.geokon.com/content/manuals/4800_Earth_Pressure_Cells.pdf.

Helwany, S. M. B., Wu, J. T. H. & Froessl, B. (2003). GRS bridge abutments-an effective means to alleviate bridge approach settlement. *Geotextiles and Geomembranes*, **21**, No. 3, 177–196.

Jiang, Y., Han, J., Parsons, R. L. & Cai, H. (2015). *Field Monitoring of MSE Walls to Investigate Secondary Reinforcement Effects*, Report. The Kansas Department of Transportation, Lawrence, KS, USA.

Morrison, K. F., Harrison, F. E., Collin, J. G., Dodds, A. & Arndt, B. (2006). *Shored Mechanically Stabilized Earth (SMSE) Wall Systems Design Guidelines*, Report No. FHWA-CFL/TD-06-001. Federal Highway Administration, Lakewood, CO, USA.

Perloff, W. H. & Baron, W. (1976). *Soil Mechanics: Principles and Applications*, John Wiley & Sons, New York, NY, USA.

Sachin, M. & Mehari, W. (2019). Geogrid reinforced soil structures reach new heights. *Geosynthetics Conference 2019*, Houston, TX, USA, pp. 387–397.

Saghebfar, M., Abu-Farsakh, M., Ardah, A., Chen, Q. & Fernandez, B. A. (2016). Performance monitoring of geosynthetic reinforced soil integrated bridge system (GRS-IBS) in Louisiana. *Geotextiles and Geomembranes*, **45**, No. 2, 34–47.

Talebi, M., Christopher, M. L. & Leshchinsky, D. (2017). Applied bearing pressure beneath a reinforced soil foundation used in a geosynthetic reinforced soil integrated bridge system. *Geotextiles and Geomembranes*, **45**, No. 6, 580–591.

Tanyu, B. F., Sabatini, P. J. & Berg, R. R. (2008). *Earth Retaining Structures-Load and Resistance Factor Design*, National Highway Institute (NHI) Course Number 132036, Document No.: FHWA-NHI-05-046. Federal Highway Administration, Washington, DC, USA.

Vennapusa, P., White, D. J., Klaiber, F. W., Wang, S. & Gieselman, H. (2012). *Geosynthetic Reinforced Soil for Low-Volume Bridge Abutments*, Report No. IHRB Project TR-621. Iowa Department of Transportation, Ames, IA, USA.

Wu, J. T. H., Lee, K. Z. Z., Helwany, S. B. & Ketchart, K. (2006). *Design and Construction Guidelines for Geosynthetic-Reinforced Soil Bridge Abutments with a Flexible Facing*, Report No. 556. National Cooperative Highway Research Program, Washington, DC, USA.

Yang, G., Liu, M., Lv, P. & Zhang, B. (2012). Geogrid-reinforced lime-treated cohesive soil retaining wall: case study and implications. *Geotextiles and Geomembranes*, **35**, 112–118.

Zheng, Y., McCartney, J. S., Shing, P. B. & Fox, P. J. (2019). Physical model tests of half-scale geosynthetic reinforced soil bridge abutments. II: dynamic loading. *Journal of Geotechnical and Geoenvironmental Engineering, ASCE*, **145**, No. 11, https://doi.org/10.1061/(ASCE)GT.1943-5606.0002158.

Zornberg, J. G., Morsy, A. M. & Mofarraj, B., Christopher, B. R., Leshchinsky, D., Han, J., Tanyu, B. F., Gebremariam, F. T., Shen, P. & Jiang, Y. (2018). *Defining the Boundary Conditions for Composite Behavior of Geosynthetic Reinforced Soil (GRS) Structures.* National Cooperative Highway Research Program (NCHRP), Project 24-41, Transportation Research Board, Washington, DC, USA.

Zornberg, J. G., Morsy, A. M., Mofarraj, B., Christopher, B. R., Leshchinsky, D., Han, J., Tanyu, B. F., Gebremariam, F. T., Shen, P. & Jiang, Y. (2019). *Proposed Refinements to Design Procedures for Geosynthetic Reinforced Soil (GRS) Structures in AASHTO LRFD Bridge Design Specifications.* National Cooperative Highway Research Program (NCHRP), Project 24-41, Transportation Research Board, Washington, DC, USA.

The Editor welcomes discussion on all papers published in Geosynthetics International. Please email your contribution to discussion@geosynthetics-international.com by 15 February 2021.